Atmos. Chem. Phys. Discuss., 13, 5729–5768, 2013
www.atmos-chem-phys-discuss.net/13/5729/2013/
doi:10.5194/acpd-13-5729-2013
© Author(s) 2013. CC Attribution 3.0 License.

Atmospheric Chemistry and Physics Discussions

This discussion paper is/has been under review for the journal Atmospheric Chemistry and Physics (ACP). Please refer to the corresponding final paper in ACP if available.

Seasonal cycle and modal structure of particle number size distribution at Dome C, Antarctica

E. Järvinen[1], A. Virkkula[1,2], T. Nieminen[1], P. P. Aalto[1], E. Asmi[2], C. Lanconelli[3], M. Busetto[3], A. Lupi[3], R. Schioppo[4], V. Vitale[3], M. Mazzola[3], T. Petäjä[1], V.-M. Kerminen[1], and M. Kulmala[1]

[1]University of Helsinki, Department of Physics, P.O. Box 64, 00014 Univ. of Helsinki, Finland
[2]Finnish Meteorological Institute, P.O. Box 503, 00560 Helsinki, Finland
[3]Institute of Atmospheric Sciences and Climate of the Italian National Research Council (ISAC-CNR), Via Gobetti, 101, 40129 Bologna, Italy
[4]ENEA-UTA Unità Tecnica Antartica, via Anguillarese 301, S.Maria di Galliera, Roma, Italy

Received: 25 January 2013 – Accepted: 14 February 2013 – Published: 4 March 2013

Correspondence to: E. Järvinen (emma.jarvinen@helsinki.fi)

Published by Copernicus Publications on behalf of the European Geosciences Union.

Abstract

We studied new particle formation and modal behavior of ultrafine aerosol particles on the high Antarctic East-Plateau at the Concordia station, Dome C (75°06′ S, 123°23′ E). Aerosol particle number size distributions were measured in the size range 10–600 nm from 14 December 2007 to 7 November 2009. We used an automatic algorithm for fitting up to three modes to the size distribution data. The total particle number concentration was low with the median of 109 cm^{-3}. There was a clear seasonal cycle in the total particle number and the volume concentrations. The concentrations were at their highest during the austral summer with the median values of 260 cm^{-3} and 0.086 $\mu m^3 cm^{-3}$, and at their lowest during the austral winter with corresponding values of 15 cm^{-3} and 0.009 $\mu m^3 cm^{-3}$. New particle formation events were determined from the size distribution data. During the measurement period, new particle formation was seen on 80 days and for 15 of these days the particle growth rates from 10 to 25 nm size could be determined. The median particle growth rate during all these events was 2.5 $nm\,h^{-1}$ and the median formation rate of 10 nm particles was 0.023 $cm^{-3}\,s^{-1}$. Most of the events were similar to those observed in other continental locations, yet also some variability in event types was observed. Exceptional features in Dome C were the winter events that occurred during dark periods, as well as the events for which the growth could be followed during several consecutive days. We called these latter events as slowly-growing events. This paper is the first one to analyze long-term size distribution data from Dome C, and also the first paper to show that new particle formation events occur in the central Antarctica.

1 Introduction

The climatic effects of atmospheric aerosol particles is tied strongly with their concentration, size distribution, chemical composition and dynamical behaviour in the atmosphere (Forster et al., 2007; Quaas et al., 2009; Ghan et al., 2012). A key process in

ACPD
13, 5729–5768, 2013

this respect is atmospheric new particle formation, including nucleation from precursor gases and subsequent growth of nucleated clusters to larger sizes (Kulmala et al., 2004; Wang and Penner, 2009; Kazil et al., 2010; Makkonen et al., 2012). The formation rate of new aerosol particles is linked closely with the gaseous sulphuric acid concentration (e.g. Kulmala et al., 2006; Petäjä et al., 2009; Kerminen et al., 2010; Sipilä et al., 2010), which can be related to sulfur dioxide originating mostly from anthropogenic sources.

The concentrations of anthropogenic aerosols have increased markedly since preindustrial times, while at the same time the concentrations of natural aerosols have remained at roughly the same level (Charlson and Wigley, 1994). Antarctica is an ideal place for studying the natural aerosol processes, since it is the continent furthest away from anthropogenic pollution sources. There is practically no vegetation, and the oceans surrounding the continent are the main source of aerosol particles (e.g. Shaw, 1988; O'Dowd et al., 1997; Asmi et al., 2010; Yu and Luo, 2010; Udisti et al., 2012) even though also some long-range transported pollutant aerosols from other continents have been observed (e.g. Fiebig et al., 2009). Studying new particle formation events in the Antarctica gives us information on natural aerosol processes and how natural processes affect the formation rate of new aerosol particles.

Aerosol number concentrations, size distributions and chemical composition have been studied at several stations around Antarctica. There exist long-term records of particle number concentrations, for instance from Neumayer (Weller et al., 2011) and South Pole (e.g. Samson, 1990) but particle number size distributions have been measured mainly during campaigns both at coastal stations (e.g. Ito, 1993; Koponen et al., 2003; Virkkula et al., 2007; Asmi et al., 2010; Pant et al., 2011; Belosi et al., 2012) and on the upper plateau at South Pole (e.g. Park et al., 2004). Hara et al. (2011) presented number size distributions and aerosol volatility measured at the Japanese Antarctic station Syowa, on the coast of Queen Maud Land in 2003–2005. The Norwegian researchers started recently long-term size distribution measurements at the Troll station, more to the inland of Queen Maud Land (Hansen et al., 2009), but there are no

ACPD
13, 5729–5768, 2013

long-term size distribution measurements from the upper plateau. The measurements presented here are the first step towards filling in this gap: particle number size distributions have been measured at the Concordia station at Dome C on the upper plateau of East Antarctica since December 2007.

New particle formation has been observed at several stations in coastal Antarctica (Ito, 1993; Koponen, 2003; Asmi et al., 2010). The motivation of this study was to observe and analyse new particle formation events in the inland Antarctica. In this work we will present seasonal variation of the particle concentrations, the modal structure of particle number size distributions, and analyses of new particle formation events during the first continuous period from December 2007 until November 2009.

2 Instrumentation and data analysis methods

2.1 Size distribution measurements

We measured particle number size distributions at the Italian–French Concordia station at Dome C (75°06′ S, 123°23′ E). The station is located on the upper plateau of East Antarctica at 3200 m above the sea level and 1100 km away from the nearest coast. The measurement period was from 14 December 2007 to 7 November 2009.

The sampling site is the same as was used by Udisti et al. (2012) and Becagli et al. (2012) for taking filter samples for chemical analyses. This sampling site is located about 1 km southwest of the station main buildings, upwind in the direction of the prevailing wind. All motorized activity is forbidden south and within 300 m north of the sampling site (Udisti et al., 2012). The northeastern direction was declared as the contaminated sector (10°–90°) due to diesel generator and motor vehicle emissions at the station. Consequently the data were omitted from further analysis, if the measured winds were from the contaminated sector. Due to contamination 6.6 percent of the measured data were removed from the analysis.

ACPD
13, 5729–5768, 2013

Snow mobiles and other traffic were active from early November to February and thus did not create major gaps to the winter measurements. However, there are minor gaps in the measured data due to power failures. Longer gaps in the data exist in early spring 2008 and in winter 2009.

Particle number size distributions in the size range 10–600 nm were measured with a Differential Mobility Particle Sizer (DMPS) that consisted of a Hauke-type medium-size DMA (Winklmayr et al., 1991) in a closed-loop arrangement and a TSI Model 3010 condensation particle counter that detects particles larger than 10 nm. The DMPS setup was similar to that used at Aboa by Virkkula et al. (2007). The time resolution of the raw data was 10 min. The size distribution data in this study is presented in the UTC time but the new particle formation plots are presented in local time (UTC + 8 h).

2.2 Data processing methods

2.2.1 Mode fitting

Log-normal modes were identified from the size distributions with an automatic algorithm (Hussein et al., 2005). This algorithm parameterizes aerosol particle number size distributions with a multi log-normal distribution function. The multi log-normal distribution function is widely in use to parameterize atmospheric aerosol particle size distributions. The algorithm used did not need a user decision for the initial input parameters, only the maximum number of fitted modes was set to be three, which is typically enough to represent atmospheric aerosol size distributions. The algorithm works by reducing the maximum number of possible modes with an overlapping test between adjacent modes. The quality of the log-normal fit is based on least-squares value between the fitted and measured size distribution. The modes found by the algorithm were numbered according to diameter from the smallest to the largest. The diameter of the fitted modes depended solely on the size distribution data. The term fitted modes is used when referring to the modes obtained by the algorithm.

ACPD
13, 5729–5768, 2013

Later in this work the terms nucleation mode, Aitken mode and accumulation mode ranges refer to the measured data in pre-selected size ranges: nucleation mode range (< 25 nm), Aitken mode range (25–100 nm) and accumulation mode range (> 100 nm) (Dal Maso et al., 2005).

2.2.2 New particle formation event classification

New particle formation event days – simply *event days* below – were determined following the procedure introduced by Dal Maso et al. (2005). We counted as an event day those days when growth of the newly formed particles could be reliably followed as well the days when growth was clearly detected but could not be followed due to for example changes in the air masses. We divided the event days into class 1 events and into class 2 events. From a class 1 event we could determine the growth rate in contrast to class 2 events. We furthermore divided the class 1 events into normal events that remind events typically observed at continental sites (for example in Hyytiälä, Finland, e.g. Dal Maso et al., 2005) and into slowly-growing events, when the growth could be followed for several days.

Event days were carefully checked to verify that the observed events were natural events and not due to contamination from the station. For this reason, the wind direction and speed were tracked two days before the event started. If the wind direction was from the polluted sector or the wind speed was lower than $2\,m\,s^{-1}$ for more than one hour during this 48-h period, or if the wind direction was from polluted sector when the event started, the event was excluded from the analysis. Examples of new particle formation events and the wind speed and direction during the events are shown in figures introduced in Sect. 3.

The lower limit of the instrument, 10 nm particle diameter, created a challenge of interpreting both the event starting time and the event duration. In addition, it was not certain, whether new particle formation actually initiated on-site or whether we detected solely an appearance of a growing mode originating from particle formation that had occurred away from our station.

ACPD
13, 5729–5768, 2013

2.2.3 Growth rate calculations

Determining growth rates was not straightforward due to the unique nature of Antarctic events and we used several methods to determine growth rate depending on the type of event. For most of the normal events the method developed by Hirsikko et al. (2005) was used for determining growth rates. This method determines the particle growth by following the size class maximum. First the times of the concentration maxima in each size class are defined. Then a line is fitted to the size class maximum times as function of size class diameter, and the slope of this line gives the growth rate. The method is limited for events in which growth can be followed to larger sizes.

For those normal events, where Hirsikko et al. (2005) method did not work, and for slowly growing events the growth rates were determined by mode-fitting method or by fitting curve to the calculated geometric mean diameter. The mode-fitting method is based on the log-normal modes fitted to each number size distribution using the algorithm of Hussein et al. (2005). The method works by selecting the geometric mean diameter of the growing nucleation mode based on visual inspection of the daily contour plots of the particle size distributions. The growth rate is then obtained by a linear least-squares fit to these selected nucleation mode mean diameters as function of time. Further details of this method can be found in Dal Maso et al. (2005), Yli-Juuti et al. (2011) and Kulmala et al. (2012). The method for calculating growth rate from geometric mean was similar to the method described above but used calculated geometric mean from measured data instead of mode data. In some cases two different methods of determining growth rate could be used for the same day and we had to choose the method that was qualitatively best. The methods used for calculating the growth rate on each event day are given in Table 3.

2.2.4 Formation rate, vapor concentration and source rate

The formation rate of nucleation mode particles (in this case particles between 10 and 25 nm) was calculated from the measured number concentration in this size range,

ACPD
13, 5729–5768, 2013

taking into account particle losses due to coagulation and condensational growth out of the size range. The formation rate of 10 nm particles, J_{10}, can be written as (Dal Maso et al., 2005)

$$J_{10} = \frac{\mathrm{d}N}{\mathrm{d}t} + \mathrm{CoagS} \cdot N + \frac{\mathrm{GR}}{\Delta d_\mathrm{p}} \cdot N \quad (1)$$

Here N is the particle number concentration of 10–25 nm particles, CoagS is the coagulation sink due to pre-existing aerosol particles and GR is the particle growth rate over the size range of width Δd_p. Coagulation sink for nucleation mode particles is calculated from the measured size distributions according to the method presented in Kulmala et al. (2012).

The condensational growth rate explained by certain vapor concentration C_v can be calculated using the formula (Nieminen et al., 2010)

$$\mathrm{GR} = \frac{2 \cdot Kn \cdot \beta}{3 \cdot \rho_\mathrm{v}} \cdot \left(\frac{8kT}{\pi}\right) \cdot \left(1 + \frac{d_\mathrm{v}}{d_\mathrm{p}}\right)^2 \cdot \left(\frac{1}{m_\mathrm{p}} + \frac{1}{m_\mathrm{v}}\right)^{1/2} \cdot m_\mathrm{v} \cdot C_\mathrm{v} \quad (2)$$

Here m_v, d_v and ρ_v are the vapor molecule mass, diameter and condensed phase density, d_p is the diameter of the growing particle and T the ambient temperature. Kn and β are the Knudsen number and the Fuchs–Sutugin transition regime correction factor for mass flux, respectively. Equation (2) can be used to calculate the vapor concentration required to explain the observed particle growth rates. Assuming molecular properties of sulphuric acid for the condensing vapor, concentration of 10^7 molecules cm^{-3} corresponds to growth rate of 0.4 nm h^{-1} for nucleation mode (10–25 nm) particles.

The source rate Q_v for the condensing vapor can be calculated from the equation describing the evolution of vapor concentration:

$$\frac{\mathrm{d}C_\mathrm{v}}{\mathrm{d}t} = Q_\mathrm{v} - \mathrm{CS} \cdot C_\mathrm{v} \quad (3)$$

ACPD
13, 5729–5768, 2013

In steady-state ($dC_v/dt = 0$) the vapor source rate is

$$Q_v = CS \cdot C_v \quad (4)$$

Here the condensation sink CS onto aerosol particles is calculated from the measured particle size distributions according to Kulmala et al. (2012).

3 Results and discussion

3.1 General features and seasonal cycle

Over 81 000 size spectra were measured during the measurement period, in which over 76 000 size spectra were used in data analysis. We used four seasons when calculating statistics: summer (December–February), autumn (March–May), winter (June–August), and spring (September–November). In summer, sunlight was present day round, whereas the winter months were completely dark. The average temperature in winter was −63 °C and in summer −36 °C.

A clear seasonal cycle of the particle number concentrations was seen in the number size distribution data (Figs. 1 and 2). The particle number concentrations were at their lowest in July and August and at the highest in January. In Fig. 1 the short peaks in particle number size distribution are mainly contamination from the station (in non-cleaned dataset). However, we observed also natural peaks in the particle number concentration, which indicated new particle formation. Altogether during the measurement period we observed 80 new particle formation days, from which we could analyze particle formation and growth rates on 15 days as explained in detail in Sect. 3.3.

After cleaning the size distribution data, the total concentration of measured particles larger than 10 nm varied from 4 to 1300 particles in cm^3 and the median total concentration was 94 particles in cm^3. The median particle concentrations in the nucleation mode range was 20 particles in cm^3, in Aitken mode range 41 particles in

ACPD
13, 5729–5768, 2013

cm^3 and in accumulation mode range 6 particles in cm^3. The geometric mean diameter of the measured particles varied from (5th and 95th percentile) 20 to 64 nm and the volume concentration varied from 0.004 to 0.140 $\mu m^3 cm^{-3}$ (median value 0.033 $\mu m^3 cm^{-3}$). The particle concentrations observed at Dome C are lower than in coastal Antarctica. For instance at Neumayer the median number concentration of 25-yr of CPC data was 258 cm^{-3} (Weller et al., 2011), 64 % higher than our measured median total concentration. Other coastal measurements in the summer show a concentration of 300–1000 cm^{-3} (Ito, 1993; Gras, 1993). At the South Pole reported aerosol concentrations are about 100–300 cm^{-3} in summer and below 20 cm^{-3} in winter (Shaw, 1988; Park et al., 2004), which are close to the mean and average values measured at Dome C (Table 1).

The seasonal cycle in particle concentrations were similar to that observed at other Antarctic sites: high concentrations in summer and low in winter. The median number concentration was 260 cm^{-3} and 15 cm^{-3} in summer and in winter, respectively (Table 1). At Neumayer the annual maximum number concentration of 1000 cm^{-3} was reported in March and the minimum number concentration of < 100 cm^{-3} was reported in June/July. Weller et al. (2011) also detected variation in diurnal cycle, but according to our measurements such variation was seen in Dome C station only in summer and in spring (Fig. 3). The daily cycle in number concentrations seen in Dome C was weaker than at Neumayer, which could indicate that the mixing of boundary layer is stronger at the coastal site.

The same seasonal cycle was also observed in volume concentration (Fig. 2). The mean volume concentration was the highest in summer, ~ 0.1 $\mu m^3 cm^{-3}$ and the lowest in winter, ~ 0.02 $\mu m^3 cm^{-3}$ (Table 1). These numbers can be compared with the mass concentrations obtained from filter and impactor samples taken from Dome C, even though not simultaneously with our measurements. Udisti et al. (2012) analyzed filter and impactor samples from December 2004 to December 2007, which is not the same period as in our work but the general level can be compared. They did not weigh the samples but analyzed them for the concentrations of major ionic constituents. In

ACPD
13, 5729–5768, 2013

addition, they did not present the total concentrations but the concentrations of sea salt and its contribution to the sum of analyzed ions for particles with $D_p < 10\,\mu m$. The 3-yr average concentration of sea-salt was $10.7\,ng\,m^{-3}$ in summer and $58.8\,ng\,m^{-3}$ in winter. The respective average contributions were 11.2 % and 84.3 % so it can be calculated that in the data of Udisti et al. (2012) the average mass concentrations were $\sim 96\,ng\,m^{-3}$ in summer and $\sim 70\,ng\,m^{-3}$ in winter. The average volume concentration calculated from our DMPS data was $0.103\,\mu m^3\,cm^{-3}$ and $0.021\,\mu m^3\,cm^{-3}$ in summer and winter, respectively (Table 1). If it is assumed that the particle density is that of water, $1\,g\,cm^{-3}$, the mass concentrations were $103\,ng\,m^{-3}$ and $21\,ng\,m^{-3}$ in summer and winter, respectively. With the density of ammonium sulfate, $1.8\,g\,cm^{-3}$, the concentrations would be $185\,ng\,m^{-3}$ in summer and $38\,ng\,m^{-3}$ in winter. The above calculations show that the order of magnitude is the same but detailed comparison needs to be done for a period when both number size distributions and chemical sampling are conducted simultaneously.

We compared the particle concentrations in nucleation, Aitken and accumulation size range. The particle number concentration of nucleation and Aitken mode range were typically similar to each other whereas accumulation mode concentrations were approximately one order of magnitude lower than in the two other modes (Fig. 1). The particle number concentrations were highest in the nucleation mode throughout the whole period, except periods in summer months during 2008 and 2009, when the particle number concentration was the highest in the Aitken mode. In summer we see the growth of newly formed particles in to the Aitken mode. The lowest particle number concentrations were usually in the accumulation mode, which indicates that the majority of the growing particles do not reach accumulation mode. The particle number concentrations in all the size classes followed the same seasonal cycle of summer maximum and winter minimum.

To further visualize the differences in the size distributions in summer and winter, simple descriptive statistic were calculated, i.e. cumulative concentrations in each size channel of the data (Fig. 4). Figure 4 shows clearly that the modes of the size

ACPD
13, 5729–5768, 2013

distributions were smaller in winter than in summer. In winter the mode of the median size distribution was at about 20 nm and in summer at about 40 nm. We also found that in summer particle number concentrations were higher in every size class.

3.2 Modal structure of measured particle size spectra

We studied the modal structure of the particle size distributions by using the automatic mode-fitting algorithm discussed above. We compared the modes calculated with the algorithm to measured particle size distribution data (Fig. 5). The cumulative sum of the fitted modes matched the measured size distribution well, both in the case where there are three modes present as well as when only one mode was observed.

We wanted to study the occurrence of the fitted modes and at which sizes the modes are fitted (median diameter of modes). If one mode was present, the median diameter of the fitted mode was 19 nm in the winter and 39 nm in the summer. When two or more modes were present particles were found in smaller sizes. This indicates that strongest new particle formation events occurred in summer and, as explained above, the growth did not reach large sizes in the accumulation mode. Also in winter when the second and the third mode had the same median values, particles were found in smaller sizes when three modes were observed than when only one or two modes were observed.

Figure 6 shows the relative frequency of the modes calculated by the automatic algorithm and how they fit to the nucleation mode, Aitken mode and the accumulation mode size range. We calculated the relative frequency by summing up the occurrence of the modes in the nucleation, Aitken and accumulation size range in each month and dividing it with the number of modes in each month. When the particle number concentration was low (in winter), most of the time only one mode was present. When the new particle formation took place or particle number concentrations were high, usually three modes were found. The automatic algorithm fitted most of the modes in nucleation mode or Aitken mode range. We found that most of the modes were in the nucleation mode range from May to August when the total concentrations were the lowest, whereas other months most of the modes were in the Aitken mode size

ACPD
13, 5729–5768, 2013

range. The occurrence of fitted modes in the accumulation mode range was the highest during winter months when nucleation was most frequently observed and the particles were also able to grow to bigger sizes. This all indicates that the particles on the high Antarctic East-Plateau air are small and are not growing very fast or at all.

3.3 New particle formation and growth

We classified the days with respect to new particle formation into class 1 event days, class 2 event days, apple events (Vana et al., 2008), undefined days and non-event days (Fig. 7). Before analysis the contamination events were excluded from the event days (Fig. 8). We observed event days mainly in the Antarctic summer, and the event frequency was peaking in November and February. In February 29 percent of the days were event days. The month with the lowest occurrence of events was July when we observed events in 5 percent of the days. Most of the events belonged to the class 2, which means that the particle growth rate could not be determined. We observed class 1 events during all the summer months and also in March, May, October and November. The highest fraction of class 1 events were observed in November, roughly one event in every tenth day. The fraction of undefined days varied from 0 to 28 percent, the highest percentage being in November. The fraction of non-event days varied from 43 to 93 percent.

To further analyze the different events, we divided the class 1 events into "normal" events and "slowly-growing" events. By normal event we mean similar kinds of events that have been observed practically all over the world in different environments (Kulmala et al., 2004), whereas slowly-growing event are characterized by the continuous and slow particle growth of up to several days. Ten of the 13 normal events (for an example see Fig. 9) were observed during the Antarctic summer. The continuous growth of the nucleated particles during several hours suggests that the new particle formation occurs in an area that is from tens of kilometers up to hundreds of kilometers wide, depending on the wind conditions. Since the distance from Dome C to the nearest

ACPD
13, 5729–5768, 2013

coastline is several hundred kilometers, this means that the newly formed particles are growing while the air masses are over the plateau of Antarctica.

Apple events took place in February, March, June, September, October and November and we observed them during 0–7 percent of the days depending on the month. In apple events nucleation occurs in a more localized area than in the class 1 events, and these locally-formed particles arrive at the measurement station after they have grown a certain time, which depends on the air mass properties. This event type has been previously shown to be typical for new particle formation in coastal regions, where this phenomenon is connected with coastal emissions following the low tide (Ehn et al., 2010). Apple events have also been observed at the near-coastal Antarctica site Aboa (Asmi et al., 2010; Kyrö et al., 2012). In our measurements, classification of apple events is somewhat uncertain, since we cannot be sure from which sizes the new-particle formation started and how the event was shaped at sizes below 10 nm.

At Dome C there were two kinds of events that have not been often observed at other locations. These were the slowly-growing events mentioned above and winter-time events (Fig. 10). From the slowly-growing events, particle growth rates could be calculated and the growth could be followed for up to three days. The winter events took place in the Antarctic winter when sunlight was not present and particle concentrations were extremely low. Some previous studies have also reported on night-time events taking place in the absence of solar radiation (e.g. Junninen et al., 2008; Suni et al., 2008), but the exact mechanisms and vapors involved are yet unclear (Ortega et al., 2012). Also the duration of the night-time events reported by Junninen et al. (2008) and Suni et al. (2008) were shorter than the winter events observed in our study. While it is possible that the particle formation in Antarctic dark winter has a connection to these night-time dark events, it seems still more likely that the mechanism in this specific environment is unique.

We studied the beginning times of the observed class 1 and class 2 events in local time. We used as a local time UTC + 8 h. About 38 % of the observed events started during morning hours (06:00–10:00), similarly to other observed events in

ACPD
13, 5729–5768, 2013

boreal forests and other surroundings. In winter two out of three events started at around 20:00, while all the other events started at 08:00. Events starting in the evening were observed also during other seasons. In summer, spring and autumn 25 %, 38 % and 36 % of the events, respectively, started after 17:00. Four nocturnal events were observed: three in spring and one in autumn.

Growth rates and statistics were calculated for all the class 1 events (Table 3) and for each event type: for normal events in the size ranges of 10–25 nm and 25–100 nm and for slowly-growing events in the size range of 10–25 nm (Fig. 11). We were unable to determine the growth rate in the size range of 25–100 nm for either slowly-growing events or winter events, since the growth could not be followed above 25 nm in those cases. The statistics were calculated season-wise, but in some seasons we observed only one or two class 2 events, so statistics for those seasons are not reliable.

The growth rate of all the class 1 events varied from 0.5 to 14 $\mathrm{nm\,h^{-1}}$ in the size range 10–25 nm, and the median growth rate was 2.5 $\mathrm{nm\,h^{-1}}$ based on 15 events (Table 3). These values are comparable to those usually observed in continental rural and clean sites (e.g. Kulmala et al., 2004; Manninen et al., 2010; Asmi et al., 2011). Most of the class 1 events were normal events. We were able to determine the growth rate statistics of normal events only for summer when the growth rate varied from 0.8 to 4.6 $\mathrm{nm\,h^{-1}}$ with the median of 2.5 $\mathrm{nm\,h^{-1}}$. In spring we were able to derive only two growth rates and in autumn only one growth rate from the total of 40 events observed during those seasons, but all being unusually high values in Antarctica. The median growth rate of normal events in the size range of 25 to 100 nm was 0.8 $\mathrm{nm\,h^{-1}}$. For the slowly-growing events the median growth rate was 1.0 $\mathrm{nm\,h^{-1}}$, indicating low concentrations of condensable gases.

The formation rates of 10 nm particles, J_{10}, of the class 1 events varied from 0.0043 to 0.11 $\mathrm{cm^{-3}\,s^{-1}}$ with the median of 0.023 $\mathrm{cm^{-3}\,s^{-1}}$ (Table 3). The median formation rate of 10 nm particle in Dome C is about an order of magnitude smaller than that measured in Aboa and more than two orders of magnitude smaller than that measured in Hyytiälä (Table 4). The value of the condensation sink varied from 0.3×10^{-4}

ACPD
13, 5729–5768, 2013

to $3.8 \times 10^{-4}\,s^{-1}$ with the median of $1.8 \times 10^{-4}\,s^{-1}$ in Dome C. These values are similar to those observed in Aboa, but about a magnitude lower than those observed in Hyytiälä (Table 4). Figure 12 shows the relation between the average values of J_{10} and CS during the class 1 events. There seems to an overall tendency of more intense new particle formation at higher values of the condensation sink. Since the condensation sink is closely related to the aerosol surface area and submicron aerosol mass concentration, this connection might suggest that the air masses having more particulate matter have also more vapors participating in new particle formation.

It is unknown which vapors condenses onto newly-formed aerosol particles and make them grow (e.g. Riipinen et al., 2011). Since sulphuric acid is very likely involved in new particle formation and early growth, we used Eq. (2) here to estimate how high sulphuric acid concentration would be needed for explaining the observed growth. The calculated vapor concentrations in the 15 class 1 events varied from 1.1 to 32×10^7 molecules cm^{-3} with the median of 5.7×10^7 molecules cm^{-3}. Mauldin et al. (2001, 2004) measured sulphuric acid concentration at the South Pole in the Antarctic summer. The median concentration was 2.7×10^5 molecules cm^{-3}. If sulphuric acid concentrations are the same magnitude in Dome C, this compound can explain only a small fraction of the particle growth rate in there.

4 Conclusions

We observed a clear seasonal cycle in the particle number concentrations, similar to that reported for other Antarctic stations. However, this study was the first one that presents the seasonal cycle of the frequency of the main three modes of the aerosol submicron number size distributions: the nucleation, Aitken and accumulation mode. An automatic algorithm was used to calculate modes from the particle size distribution data. The automatically-fitted modes were located mainly in the nucleation and Aitken size ranges. Overall, the great majority of the particles were found in sizes below

ACPD
13, 5729–5768, 2013

100 nm of particle diameter, which is probably due to small amount of condensable vapours.

New particle formation events were observed every month, but this phenomenon was most frequent during the summer months. A new finding was winter events, which was not expected, as there is no sunlight during winter. The apparent growth of winter events was limited and we were not able to determine growth rate of these events at sizes below 25 nm. Another interesting finding were the slowly-growing event for which continuous particle growth was evident during several consecutive days.

The median growth rate of class 1 events in the size range of 10 to 25 nm was 2.5 $nm\,h^{-1}$. Asmi et al. (2010) analyzed new particle formation events observed at the Finnish Antarctic station Aboa and found that the range of the growth rates was 1.3–2.5 $nm\,h^{-1}$ in the same size range. So, it seems there is not a very significant difference in the growth rates between these two sites. This is somewhat surprising, considering that Aboa is close to the ocean that is the source of most condensable compounds in the region, whereas Dome C is high above the ocean and far away from the coast. The frequency of event days in January was 22 in Dome C which is very similar to that observed in Aboa Station (Asmi et al., 2010).

Analyzing the new particle formation events and calculating growth rates was not straight forward. Our size-distribution measurements started from 10 nm, which means that the beginning of the nucleation was not detected. In order to better classify new particle formation events and calculate growth rates, it is crucial to be able to measure particle properties at sizes smaller than 10 nm.

Acknowledgements. This research was supported by the Academy of Finland (Center of Excellence program, project number 127534, and Finnish Antarctic Research Program, decision nrs. 264375 and 264390), by the Nordic Top-level Research Initiative (TRI) Cryosphere-Atmosphere Interactions in a Changing Arctic Climate (CRAICC) and by the Italian "Programma Nazionale di Ricerche in Antartide" (PNRA) and developed as a sub-project 2010/A3.05 "Effetti radiativi diretti di aerosol e nubi sul clima alle alte latitudini: una prospettiva bipolare (DECA-POL)".

ACPD
13, 5729–5768, 2013

Meteorological data used in this study were obtained from the "RMO – Osservatorio Climatologico" of the Programma Nazionale di Ricerche in Antartide (PNRA) (http://www.climantartide.it).

References

Asmi, E., Frey, A., Virkkula, A., Ehn, M., Manninen, H. E., Timonen, H., Tolonen-Kivimäki, O., Aurela, M., Hillamo, R., and Kulmala, M.: Hygroscopicity and chemical composition of Antarctic sub-micrometre aerosol particles and observations of new particle formation, Atmos. Chem. Phys., 10, 4253–4271, doi:10.5194/acp-10-4253-2010, 2010.

Asmi, E., Kivekäs, N., Kerminen, V.-M., Komppula, M., Hyvärinen, A.-P., Hatakka, J., Viisanen, Y., and Lihavainen, H.: Secondary new particle formation in Northern Finland Pallas site between the years 2000 and 2010, Atmos. Chem. Phys., 11, 12959–12972, doi:10.5194/acp-11-12959-2011, 2011.

Becagli, S., Scarchilli, C., Traversi, R., Dayan, U., Severi, M., Frosini, D., Vitale, V., Mazzola, M., Lupi, A., Nava, S., and Udisti, R.: Study of present-day sources and transport processes affecting oxidised sulphur compounds in atmospheric aerosols at Dome C (Antarctica) from year-round sampling campaigns, Atmos. Environ., 52, 98–108, 2012.

Belosi, F., Contini, D., Donateo, A., Santachiara, G., and Prodi, F.: Aerosol size distribution at Nansen Ice Sheet Antarctica, Atmos. Res., 107, 42–50, 2012.

Charlson, R. J. and Wigley, T. M. L.: Sulphate aerosol and climatic change, Sci. Am., 270, 48–57, 1994.

Dal Maso, M., Kulmala, M., Riipinen, I., Wagner, R., Hussein, T., Aalto, P. P., and Lehtinen, K. E. J.: Formation and growth of fresh atmospheric aerosols: eight years of aerosol size distribution data from SMEAR II, Hyytiälä, Finland, Boreal Environ. Res., 10, 323–336, 2005.

Ehn, M., Vuollekoski, H., Petäjä, T., Kerminen, V.-M., Vana, M., Aalto, P. P., de Leeuw, G., Ceburnis, D., Dupuy, R., O'Dowd, C. D., and Kulmala, M.: Growth rates during coastal and marine new particle formation in western Ireland, J. Geophys. Res., 115, D18218, doi:10.1029/2010JD014292, 2010.

ACPD
13, 5729–5768, 2013

Fiebig, M., Lunder. C. R., and Stohl, A.: Tracing biomass burning aerosol from South America to Troll research station, Antarctica, Geophys. Res. Lett., 36, L14815, doi:10.1029/2009GL038531, 2009.

Forster, P., Ramaswamy, V., Artaxo, P., Berntsen, T., Betts, R., Fahey, D. W., Haywood, J., Lean, J., Lowe, D. C., Myhre, G., Nganga, J., Prinn, R., Raga, G., Schulz, M., and Van Dorland, R.: Cheanges in atmospheric constituents and in radiative forcing, in: Climate Change 2007: The Physical Science Basis. Contribution of Working Group I to the Fourth Assessment Report of the Intergovernmental Panel on Climate Change, edited by: Solomon, S., Qin, D., Manning, M., Chen, Z., Marquis, M., Averyt, K. B., Tignor, M., and Miller, H. L., Cambridge University Press, Cambridge, UK and New York, NY, USA, 2007.

Ghan, S. J., Liu, X., Easter, R. C., Zaveri, R., Rasch, P. J., and Yoon, J.-H.: Toward a minimal representation of aerosols in climate models: comparative decomposition of aerosol direct, semidirect, and indirect effects, J. Climate, 25, 6461–6476, 2012.

Gras, J. L.: Condensation nucleus size distribution at Mawson, Antarctica: microphysics and chemistry, Atmos. Environ., 27, 1417–1425, 1993.

Hansen, G., Aspmo, K., Berg, T., Edvardsen, K., Fiebig, M., Kallenborn, R., Krognes, T., Lunder, C., Stebel, K., Schmidbauer, N., Solberg, S., and Yttri, K. E.: Atmospheric monitoring at the Norwegian Antarctic station Troll: measurement programme and first results, Polar Res., 28, 353–363, 2009.

Hara, K., Osada, K., Nishita-Hara, C., Yabuki, M., Hayashi, M., Yamanouchi, T., Wada, M., and Shiobara, M.: Seasonal features of ultrafine particle volatility in the coastal Antarctic troposphere, Atmos. Chem. Phys., 11, 9803–9812, doi:10.5194/acp-11-9803-2011, 2011.

Hirsikko, A., Laakso, L., Hõrrak, U., Aalto, P. P., Kerminen, V.-M., and Kulmala, M.: Annual and size dependent variation of growth rates and ion concentrations in boreal forest, Boreal Environ. Res., 10, 357–369, 2005.

Hussein, T., Dal Maso, M., Petäjä, T., Koponen, I., Paatero, P., Aalto, P., Hämeri, K., and Kulmala M.: Evaluation of an automatic algorithm for fitting the particle number size distributions, Boreal Environ. Res., 10, 337–355, 2005.

Ito, T.: Size distribution of Antarctic submicron aerosols, Tellus B, 45, 145–159, 1993.

Junninen, H., Hulkkonen, M., Riipinen, I., Nieminen, T., Hirsikko, A., Suni, T., Boy, M., Lee, S.-H., Vana, M., Tammet, H., Kerminen, V.-M., and Kulmala, M.: Observations on nocturnal growth of atmospheric clusters, Tellus B, 60, 365–371. 2008.

ACPD
13, 5729–5768, 2013

Kazil, J., Stier, P., Zhang, K., Quaas, J., Kinne, S., O'Donnell, D., Rast, S., Esch, M., Ferrachat, S., Lohmann, U., and Feichter, J.: Aerosol nucleation and its role for clouds and Earth's radiative forcing in the aerosol-climate model ECHAM5-HAM, Atmos. Chem. Phys., 10, 10733–10752, doi:10.5194/acp-10-10733-2010, 2010.

Kerminen, V.-M., Petäjä, T., Manninen, H. E., Paasonen, P., Nieminen, T., Sipilä, M., Junninen, H., Ehn, M., Gagné, S., Laakso, L., Riipinen, I., Vehkamäki, H., Kurten, T., Ortega, I. K., Dal Maso, M., Brus, D., Hyvärinen, A., Lihavainen, H., Leppä, J., Lehtinen, K. E. J., Mirme, A., Mirme, S., Hõrrak, U., Berndt, T., Stratmann, F., Birmili, W., Wiedensohler, A., Metzger, A., Dommen, J., Baltensperger, U., Kiendler-Scharr, A., Mentel, T. F., Wildt, J., Winkler, P. M., Wagner, P. E., Petzold, A., Minikin, A., Plass-Dülmer, C., Pöschl, U., Laaksonen, A., and Kulmala, M.: Atmospheric nucleation: highlights of the EUCAARI project and future directions, Atmos. Chem. Phys., 10, 10829–10848, doi:10.5194/acp-10-10829-2010, 2010.

Koponen, I., Virkkula, A., Hillamo, R., Kerminen, V.-M., and Kulmala, M.: Number size distributions and concentrations of the continental summer aerosols in Queen Maud Land, Antarctica, J. Geophys. Res., 108, 4587, doi:10.1029/2003JD003614, 2003.

Kulmala, M., Vehkamäki, H., Petäjä, T., Dal Maso, M., Lauri, A., Kerminen, V.-M., Birmili, W., and McMurry, P. H.: Formation and growth rates of ultrafine atmospheric particles: a review of observations, J. Aerosol Sci., 35, 143–176. 2004.

Kulmala, M., Lehtinen, K. E. J., and Laaksonen, A.: Cluster activation theory as an explanation of the linear dependence between formation rate of 3nm particles and sulphuric acid concentration, Atmos. Chem. Phys., 6, 787–793, doi:10.5194/acp-6-787-2006, 2006.

Kulmala, M., Petäjä, T., Nieminen, T., Sipilä, M., Manninen, H. E., Lehtipalo, K., Dal Maso, M., Aalto, P. P., Junninen, H., Paasonen, P., Riipinen, I., Lehtinen, K. E. J., Laaksonen, A., and Kerminen, V.-M.: Measurement of the nucleation of atmospheric aerosol particles, Nat. Protoc., 7, 1651–1667, doi:10.1038/nprot.2012.091, 2012.

Kyrö, E.-M., Kerminen, V.-M., Virkkula, A., Dal Maso, M., Parshintsev, J., Ruíz-Jimenez, J., Forsström, L., Manninen, H. E., Riekkola, M.-L., Heinonen, P., and Kulmala, M.: Antarctic new particle formation from continental biogenic precursors, Atmos. Chem. Phys. Discuss., 12, 32741–32794, doi:10.5194/acpd-12-32741-2012, 2012.

Makkonen, R., Asmi, A., Kerminen, V.-M., Boy, M., Arneth, A., Hari, P., and Kulmala, M.: Air pollution control and decreasing new particle formation lead to strong climate warming, Atmos. Chem. Phys., 12, 1515–1524, doi:10.5194/acp-12-1515-2012, 2012.

ACPD
13, 5729–5768, 2013

Manninen, H. E., Nieminen, T., Asmi, E., Gagné, S., Häkkinen, S., Lehtipalo, K., Aalto, P., Vana, M., Mirme, A., Mirme, S., Hõrrak, U., Plass-Dülmer, C., Stange, G., Kiss, G., Hoffer, A., Törő, N., Moerman, M., Henzing, B., de Leeuw, G., Brinkenberg, M., Kouvarakis, G. N., Bougiatioti, A., Mihalopoulos, N., O'Dowd, C., Ceburnis, D., Arneth, A., Svenningsson, B., Swietlicki, E., Tarozzi, L., Decesari, S., Facchini, M. C., Birmili, W., Sonntag, A., Wiedensohler, A., Boulon, J., Sellegri, K., Laj, P., Gysel, M., Bukowiecki, N., Weingartner, E., Wehrle, G., Laaksonen, A., Hamed, A., Joutsensaari, J., Petäjä, T., Kerminen, V.-M., and Kulmala, M.: EUCAARI ion spectrometer measurements at 12 European sites – analysis of new particle formation events, Atmos. Chem. Phys., 10, 7907–7927, doi:10.5194/acp-10-7907-2010, 2010.

Mauldin III, R., Eisele, F., Tanner, D., Kosciuch, E., Shetter, R., Lefer, B., Hall, S., Nowak, J., Buhr, M., Chen, G., Wang, P., and Davis, D.: Measurements of OH, H_2SO_4, and MSA at the South Pole during ISCAT, Geophys. Res. Lett., 28, 3629–3632, 2001

Mauldin, R. L., Kosciuch, E., Henry, B., Eisele, F., Shetter, R., Lefer, B., Chen, G., Davis, D., Bandy, A., and Thornton, D.: Measurements of OH, $HO_2 + RO_2$, H_2SO_4, and MSA at the South Pole during ISCAT 2000, Atmos. Environ., 38, 5423–5437, 2004.

Nieminen, T., Lehtinen, K. E. J., and Kulmala, M.: Sub-10 nm particle growth by vapor condensation – effects of vapor molecule size and particle thermal speed, Atmos. Chem. Phys., 10, 9773–9779, doi:10.5194/acp-10-9773-2010, 2010.

O'Dowd, C. D., Lowe, J. A., Smith, M. H., Davison, B., Hewitt, C. N., and Harrison, R. M.: Biogenic sulphur emissions and inferred non-sea-salt-sulphate cloud condensation nuclei in and around Antarctica, J. Geophys. Res., 102, 12839–12854, 1997.

Ortega, I. K., Suni, T., Boy, M., Grönholm, T., Manninen, H. E., Nieminen, T., Ehn, M., Junninen, H., Hakola, H., Hellén, H., Valmari, T., Arvela, H., Zegelin, S., Hughes, D., Kitchen, M., Cleugh, H., Worsnop, D. R., Kulmala, M., and Kerminen, V.-M.: New insights into nocturnal nucleation, Atmos. Chem. Phys., 12, 4297–4312, doi:10.5194/acp-12-4297-2012, 2012.

Park, J., Sakurai, H., Vollmers, K., and McMurry, P. H.: Aerosol size distributions measured at the South Pole during ISCAT, Atmos. Environ., 38, 5493–5500, 2004.

Pant, V., Siingh, D., and Kamra, A. K.: Size distribution of atmospheric aerosols at Maitri, Antarctica, Atmos. Environ., 45, 5138–5149, 2011.

Petäjä, T., Mauldin, III, R. L., Kosciuch, E., McGrath, J., Nieminen, T., Paasonen, P., Boy, M., Adamov, A., Kotiaho, T., and Kulmala, M.: Sulfuric acid and OH concentrations in a boreal forest site, Atmos. Chem. Phys., 9, 7435–7448, doi:10.5194/acp-9-7435-2009, 2009.

ACPD
13, 5729–5768, 2013

Quaas, J., Ming, Y., Menon, S., Takemura, T., Wang, M., Penner, J. E., Gettelman, A., Lohmann, U., Bellouin, N., Boucher, O., Sayer, A. M., Thomas, G. E., McComiskey, A., Feingold, G., Hoose, C., Kristjánsson, J. E., Liu, X., Balkanski, Y., Donner, L. J., Ginoux, P. A., Stier, P., Grandey, B., Feichter, J., Sednev, I., Bauer, S. E., Koch, D., Grainger, R. G., Kirkevåg, A., Iversen, T., Seland, Ø., Easter, R., Ghan, S. J., Rasch, P. J., Morrison, H., Lamarque, J.-F., Iacono, M. J., Kinne, S., and Schulz, M.: Aerosol indirect effects – general circulation model intercomparison and evaluation with satellite data, Atmos. Chem. Phys., 9, 8697–8717, doi:10.5194/acp-9-8697-2009, 2009.

Riipinen, I., Pierce, J. R., Yli-Juuti, T., Nieminen, T., Häkkinen, S., Ehn, M., Junninen, H., Lehtipalo, K., Petäjä, T., Slowik, J., Chang, R., Shantz, N. C., Abbatt, J., Leaitch, W. R., Kerminen, V.-M., Worsnop, D. R., Pandis, S. N., Donahue, N. M., and Kulmala, M.: Organic condensation: a vital link connecting aerosol formation to cloud condensation nuclei (CCN) concentrations, Atmos. Chem. Phys., 11, 3865–3878, doi:10.5194/acp-11-3865-2011, 2011.

Samson, J. A., Barnard, S. C., Obremski, J. S., Riley, D. C., Black, J. J., and Hogan, A. W.: On the systematic variation in surface aerosol concentration at the South Pole, Atmos. Res., 25, 385–396, 1990.

Shaw, G. E.: Antarctic aerosols: a review, Rev. Geophys., 26, 89–112, 1988.

Sipilä, M., Berndt, T., Petäjä, T., Brus, D., Vanhanen, J., Stratmann, F., Petakoski, J., Mauldin, L., Hyvärinen, A.-P., Lihavainen, H., and Kulmala, M.: The Role of Sulphuric Acid in Atmospheric Nucleation, Science, 327, 1243–1246, 2010.

Suni, T., Kulmala, M., Hirsikko, A., Bergman, T., Laakso, L., Aalto, P. P., Leuning, R., Cleugh, H., Zegelin, S., Hughes, D., van Gorsel, E., Kitchen, M., Vana, M., Hõrrak, U., Mirme, S., Mirme, A., Sevanto, S., Twining, J., and Tadros, C.: Formation and characteristics of ions and charged aerosol particles in a native Australian Eucalypt forest, Atmos. Chem. Phys., 8, 129–139, doi:10.5194/acp-8-129-2008, 2008.

Udisti, R., Dayan, U., Becagli, S., Busetto, M., Frosini, D., Legrand, M., Lucarelli, F., Preunkert, S., Severi, M., Traversi, R., Vitale, V.: Sea spray aerosol in central Antarctica. Present atmospheric behaviour and implications for paleoclimatic reconstructions, Atmos. Environ., 52, 109–120, 2012.

Vana, M., Ehn, M., Petäjä, T., Vuollekoski, H., Aalto, P., De Leeuw, G., Ceburnis, D., O'Dowd, C. D., and Kulmala, M.: Characteristic features of air ions at Mace Head on the west coast of Ireland, Atmos. Res., 90, 278–286, 2008.

ACPD
13, 5729–5768, 2013

Virkkula, A., Hirsikko, A., Vana, M., Aalto, P., Hillamo, R., and Kulmala M.: Charged particle size distribution and analysis of particle formation events at the Finnish Antarctic research station Alboa, Boreal Environ. Res., 12, 397–408, 2007.

Wang, M. and Penner, J. E.: Aerosol indirect forcing in a global model with particle nucleation, Atmos. Chem. Phys., 9, 239–260, doi:10.5194/acp-9-239-2009, 2009.

Weller, R., Minikin, A., Wagenbach, D., and Dreiling, V.: Characterization of the inter-annual, seasonal, and diurnal variations of condensation particle concentrations at Neumayer, Antarctica, Atmos. Chem. Phys., 11, 13243–13257, doi:10.5194/acp-11-13243-2011, 2011.

Winklmayr, W., Reischl, G. P., Lindner, A. O., and Berner, A.: New electromobility spectrometer for the measurement of aerosol size distributions in the size range from 1 to 1000 nm, J. Aerosol Sci., 22, 289–296, 1991.

Yli-Juuti, T., Nieminen, T., Hirsikko, A., Aalto, P. P., Asmi, E., Hõrrak, U., Manninen, H. E., Patokoski, J., Dal Maso, M., Petäjä, T., Rinne, J., Kulmala, M., and Riipinen, I.: Growth rates of nucleation mode particles in Hyytiälä during 2003–2009: variation with particle size, season, data analysis method and ambient conditions, Atmos. Chem. Phys., 11, 12865–12886, doi:10.5194/acp-11-12865-2011, 2011.

Yu, F. and Luo, G.: Oceanic dimethyl sulfide emission and new particle formation around the coast of Antarctica: a modeling study of seasonal variations and comparison with measurements, Atmosphere, 1, 34–50, 2010.

ACPD
13, 5729–5768, 2013

Table 1. Descriptive statistics of the total particle number concentration, geometric mean diameter and its geometric standard deviation, the particle volume concentration, modal mean diameters and their geometric standard devation, and growth rates during the four seasons.

				Percentile		
	N	Mean	Std	95 %	50 %	5 %
			Winter			
Total concentration	18 313	20.2	37.4	40.5	15.4	4.27
Geometric mean diameter [nm]	19 005	39.4	19.3	71.1	34.2	19.6
Geometric std of diameter	19 005	2.27	0.30	2.71	2.25	1.92
Volume concentration [$\mu m^3\,cm^{-3}$]	19 005	0.021	0.091	0.046	0.009	0.002
Diameter of mode 1 [nm]	16 595	29.1	30.2	85.5	18.8	9.00
Diameter of mode 2 [nm]	3740	34.7	40.9	98.7	23.3	9.00
Diameter of mode 3 [nm]	231	64.6	61.6	213	46.3	9.00
Width of mode 1	16 595	1.62	1.33	4.08	1.19	1.01
Width of mode 2	3740	2.00	1.26	4.30	1.69	1.02
Width of mode 3	231	1.77	0.97	4.22	1.38	1.07
GR 10–25 nm [$nm\,h^{-1}$]	0	–	–	–	–	–
GR 25–600 nm [$nm\,h^{-1}$]	1	0.500	–	0.500	0.500	0.500
GR from growth limited events	0	–	–	–	–	–
			Summer			
Total concentration	20 526	305	179	623	260	150
Geometric mean diameter [nm]	22 531	41.6	11.2	62.4	41.1	24.7
Geometric std of diameter	22 531	1.97	0.16	2.21	1.99	1.70
Volume concentration [$\mu m^3\,cm^{-3}$]	22 531	0.103	0.148	0.184	0.086	0.051
Diameter of mode 1 [nm]	21 643	40.2	19.6	74.9	38.5	9.00
Diameter of mode 2 [nm]	11 603	61.0	38.1	124	58.7	9.00
Diameter of mode 3 [nm]	6507	57.9	46.2	142	41.7	9.00
Width of mode 1	21 643	1.92	0.590	2.67	1.85	1.35
Width of mode 2	11 603	1.63	0.460	2.43	1.52	1.25
Width of mode 3	6507	1.58	0.480	2.35	1.47	1.19
GR 10–25 nm [nm h1 – 1]	10	3.37	2.34	9.01	2.79	0.792
GR 25–600 nm [$nm\,h^{-1}$]	7	0.640	0.410	1.13	0.780	0.210
GR from growth limited events	0	–	–	–	–	–

ACPD
13, 5729–5768, 2013

Table 1. Continued.

	N	Mean	Std	Percentile 95 %	50 %	5 %
			Autumn			
Total concentration	16 957	131	145	421	87.1	24.0
Geometric mean diameter [nm]	18 467	35.4	11.3	55.5	33.7	20.5
Geometric std of diameter	18 467	2.03	0.140	2.26	2.03	1.80
Volume concentration [$\mu m^3\,cm^{-3}$]	18 467	0.043	0.239	0.080	0.024	0.007
Diameter of mode 1 [nm]	17 843	32.4	21.3	76.5	29.7	9.00
Diameter of mode 2 [nm]	7791	48.5	31.9	104	40.3	9.00
Diameter of mode 3 [nm]	2772	46.3	37.4	110	35.0	9.00
Width of mode 1	17843	2.15	0.840	3.57	2.00	1.36
Width of mode 2	7791	1.79	0.580	2.96	1.60	1.25
Width of mode 3	2772	1.65	0.420	2.50	1.54	1.20
GR 10–25 nm [$nm\,h^{-1}$]	1	10.1	–	10.1	10.1	10.1
GR 25–600 nm [$nm\,h^{-1}$]	1	0.230	–	0.230	0.230	0.230
GR from growth limited events	2	1.26	0.050	1.29	1.26	1.22
			Spring			
Total concentration	20 351	138	176	457	85.8	17.9
Geometric mean diameter [nm]	19 005	34.5	16.4	66.2	29.8	15.8
Geometric std of diameter	21 667	1.99	0.250	2.46	1.95	1.66
Volume concentration [$\mu m^3\,cm^{-3}$]	21 670	0.057	0.220	0.098	0.030	0.007
Diameter of mode 1 [nm]	19 713	32.4	27.4	91.2	24.0	9.00
Diameter of mode 2 [nm]	11 084	38.3	28.1	93.3	30.0	9.00
Diameter of mode 3 [nm]	3649	40.4	36.4	113	34.5	9.00
Width of mode 1	19 713	1.86	0.830	3.48	1.62	1.05
Width of mode 2	11 084	1.75	0.690	2.94	1.56	1.16
Width of mode 3	3649	1.75	0.650	2.93	1.56	1.20
GR 10–25 nm [$nm\,h^{-1}$]	2	13.3	1.13	14.1	13.3	12.5
GR 25–600 nm [$nm\,h^{-1}$]	2	3.30	3.17	5.32	3.30	1.29
GR from growth limited events	1	0.490	–	0.490	0.490	0.490

ACPD
13, 5729–5768, 2013

Table 2. Descriptive statistics for data that came from the polluted sector.

				Percentile		
	N	Mean	Std	95 %	50 %	5 %
Total concentration [cm^{-3}]	5412	910	4250	2620	245	18.2
Geometric mean diameter [nm]	5411	37.1	16.2	62.2	34.7	18.4
Geometric std of diameter	5411	2.05	0.260	2.48	2.04	1.68
Volume concentration [10^{-19} μm^3 cm^{-3}]	5413	0.210	0.634	0.941	0.070	0.008

ACPD
13, 5729–5768, 2013

Table 3. Particle growth rates (GR) in the 10–25 nm size range, the derived formation rate (J_{10}) and vapor concentrations (C_V) required to explain the observed growth (the vapor is assumed to have properties of sulphuric acid) and condensation sink (CS) values during the particle formation. The methods used to determine growth rate were to fit a curve to the geometric mean diameter (A), to use the method presented by Hirsikko et al. (2005) (B), and to fit a curve to calculated mode data (C).

Date	Method	GR ($nm\,h^{-1}$)	J_{10} ($cm^{-3}\,s^{-1}$)	C_V ($10^7\,molec\,cm^{-3}$)	CS ($10^{-4}\,s^{-1}$)
9 Jan 2008	B	4.6	2.3×10^{-2}	10.5	2.1
10 Jan 2008	B	2.4	2.0×10^{-2}	5.5	3.8
26 Feb 2008	B	3.4	2.2×10^{-2}	7.9	1.7
3 Mar 2008	B	10.1	8.4×10^{-2}	23.3	1.9
9 May 2008	A	1.3	1.2×10^{-3}	3.0	0.3
3 Oct 2008	A	0.5	2.2×10^{-3}	1.1	0.3
29 Nov 2008	B	12.5	8.3×10^{-2}	28.8	1.7
29 Nov 2008	B	14.1	1.1×10^{-1}	32.5	2.2
11 Dec 2008	C	4.6	3.0×10^{-2}	10.6	2.3
20 Dec 2008	C	0.8	5.3×10^{-2}	1.8	2.5
23 Dec 2008	C	3.1	1.6×10^{-2}	7.1	1.8
30 Jan 2009	B	1.6	4.1×10^{-2}	3.6	2.5
22 Feb 2009	B	1.7	4.3×10^{-3}	3.9	1.0
24 Feb 2009	B	2.5	1.7×10^{-2}	5.7	1.7
11 Mar 2009	B	1.2	7.1×10^{-2}	2.8	1.5
Average		4.3	3.8×10^{-2}	9.9	1.8
Median		2.5	2.3×10^{-2}	5.7	1.8
Std		4.4	3.4×10^{-2}	10.0	0.9

ACPD
13, 5729–5768, 2013

Table 4. The comparison of growth rate (GR), formation rate (J_{10}) and condensation sink (CS) between Dome C, Aboa and Hyytiälä. The Aboa values represent the medians and ranges during the new particle formation events in January, 2010 (Kyrö et al., 2012). The GR values from Hyytiälä are the median and 10th to 90th percentile range of 809 new particle formation events, the value of CS value is the geometric mean of CS during these events, and J_{10} represents the median 10 nm particle formation rate (Dal Maso et al., 2007).

	Dome C	Aboa	Hyytiälä
GR ($nm\,h^{-1}$)	2.5	5.5 (1.8–8.8)	2.5 (1.1–5.3)
J_{10} ($cm^{-3}\,s^{-1}$)	0.023	0.2 (0.003–0.3)	0.4
CS (s^{-1})	1.8×10^{-4}	4.0×10^{-4}	1.7×10^{-3}

ACPD
13, 5729–5768, 2013

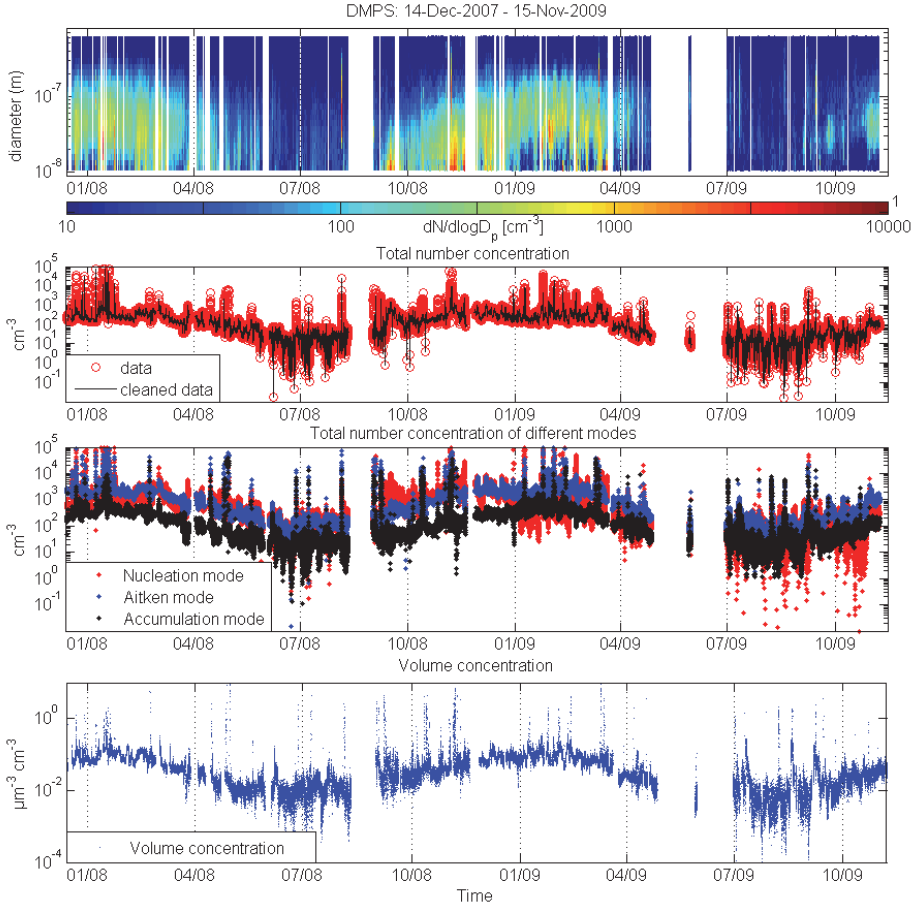

Fig. 1. Time series of the particle number size distribution, total particle number concentration, total particle number concentrations in the nucleation, Aitken mode and accumulation mode size ranges, and the total particle volume concentration.

ACPD
13, 5729–5768, 2013

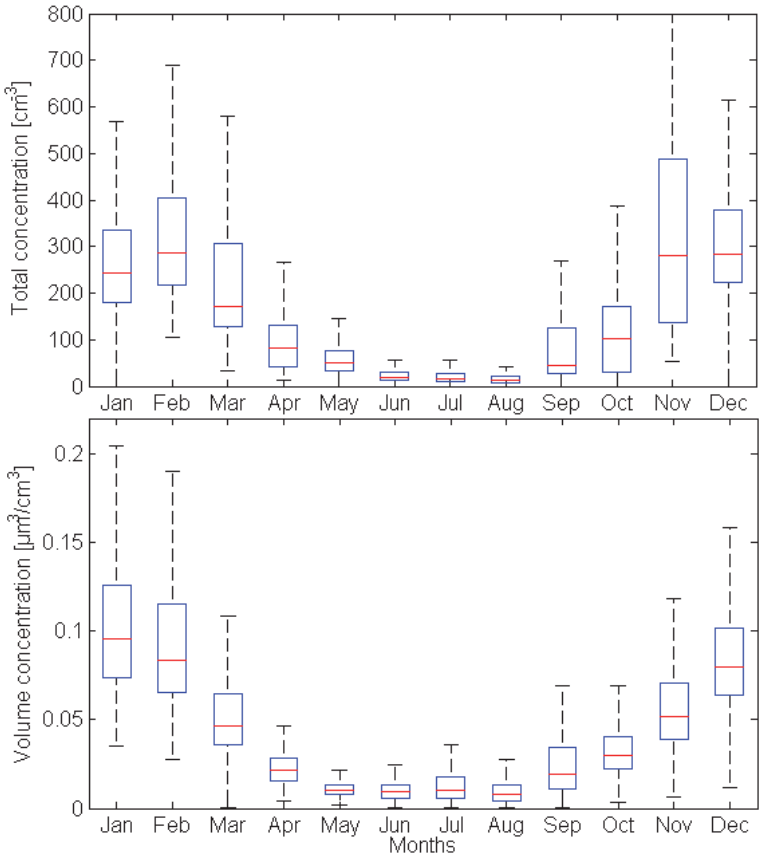

Fig. 2. The annual cycle of total number concentration (upper panel) and volume concentration (lower panel). The red bars present the median value of volume concentration, the blue box the 25th and 75th percentiles and the black bars the 5th and 95th percentiles.

ACPD
13, 5729–5768, 2013

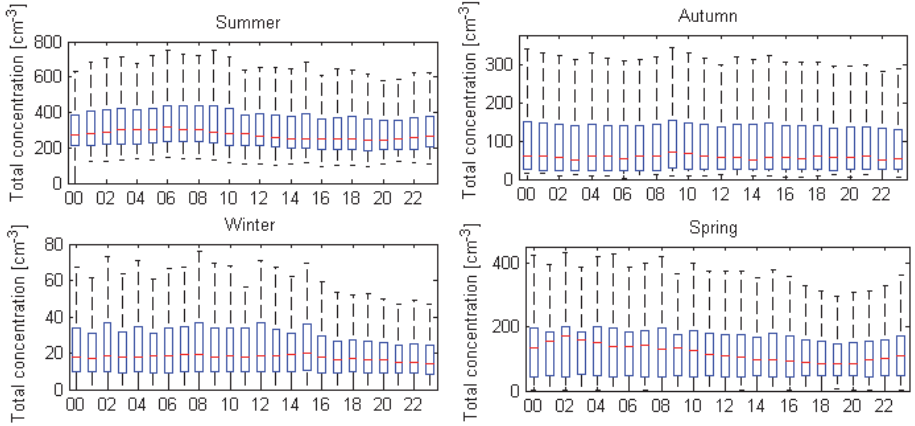

Fig. 3. The diurnal cycle of total number concentration in each season. Red bars present the median value of total concentration, blue box the 25th and 75th percentile and black bars the 5th and 95th percentile.

ACPD
13, 5729–5768, 2013

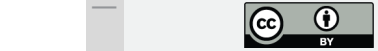

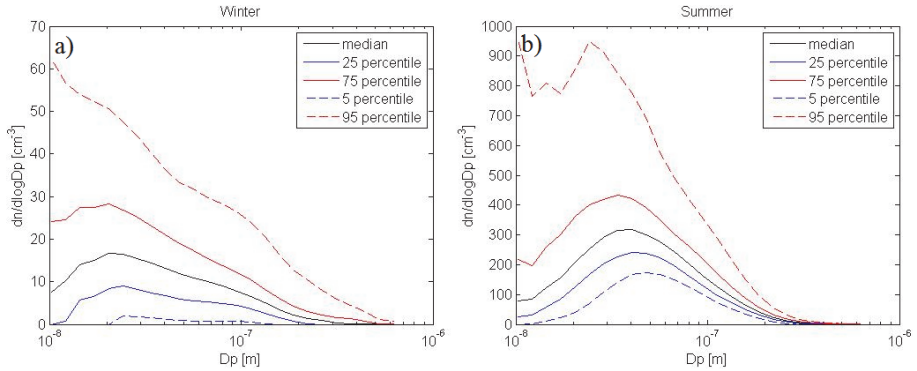

Fig. 4. The normalized particle number size distribution. Black line represents the median normalized concentration, solid blue line the 25th percentile, dashed blue line the 5th percentile, solid red line the 75 percentile and dashed red line the 95 percentile. **(a)** takes account winter months (June, July, August) and **(b)** summer months (December, January, February).

ACPD
13, 5729–5768, 2013

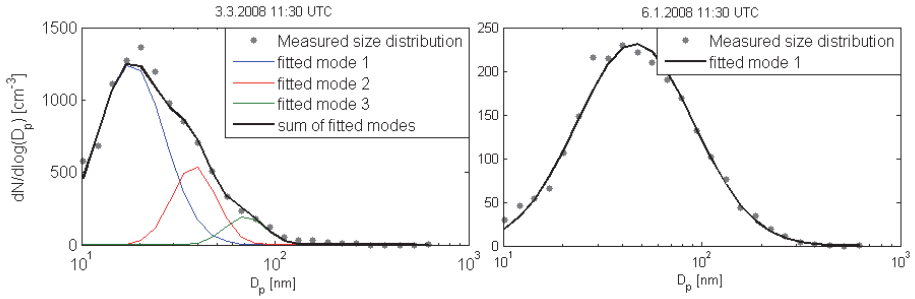

Fig. 5. Measured particle number size distribution (grey dots) and calculated modes with mode fitting algorithm (Hussein et al., 2005). On 3 March 2008, three modes were found and on 6 January 2008 one mode was found.

ACPD
13, 5729–5768, 2013

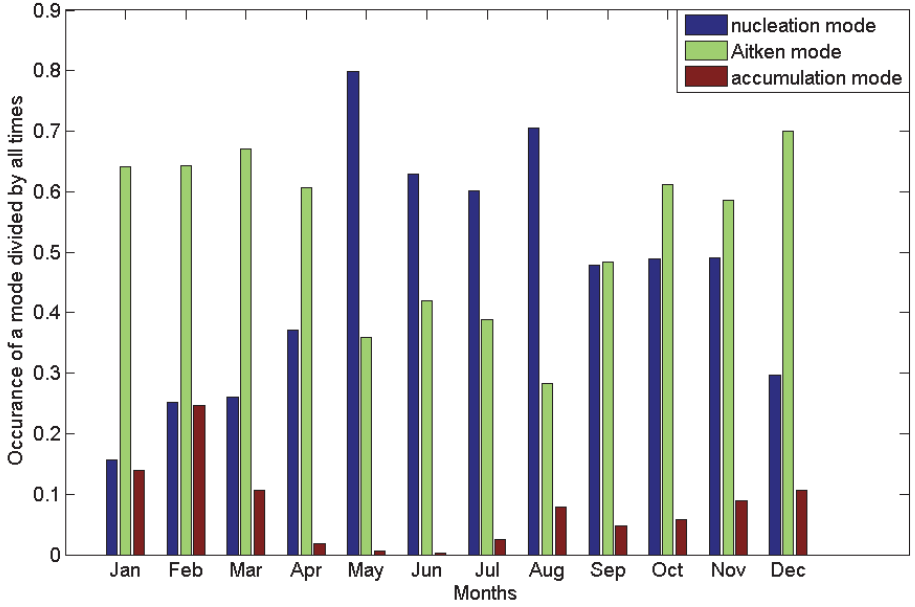

Fig. 6. Fraction of times, when one or more modes were found in the nucleation, Aitken or accumulation mode size ranges. If two or more modes were found in the same size range, the fractions of modes were added together.

ACPD
13, 5729–5768, 2013

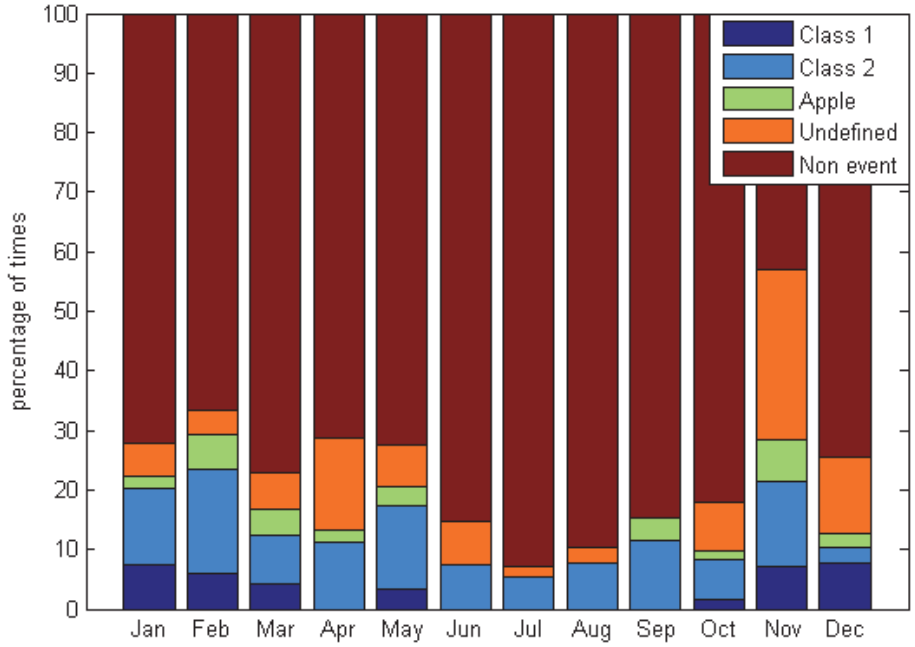

Fig. 7. Event classification from the whole period. Monthly percentage of class 1 event days (dark blue), class 2 event days (light blue), undefined days (yellow) and non-event days (brown).

ACPD
13, 5729–5768, 2013

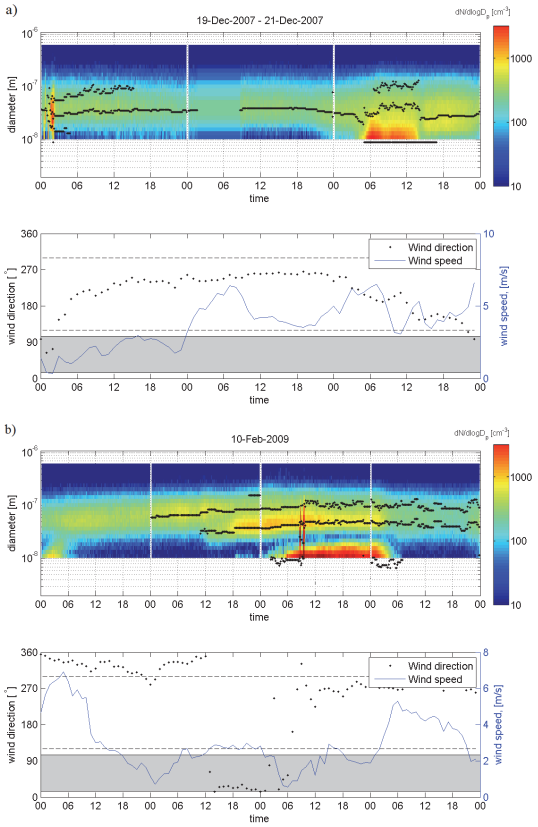

Fig. 8. Examples of quality check of the event analysis. In both cases the upper panel shows particle number size distributions during two days before an event and the event day, and the lower panel represents the wind direction (dots) and wind speed (blue line) from the same period. The shaded area represents the contaminated wind direction sector. Dashed lines rule the area of wind direction where most of the clean events come. Event **(a)** was a real event and event **(b)** was excluded.

ACPD
13, 5729–5768, 2013

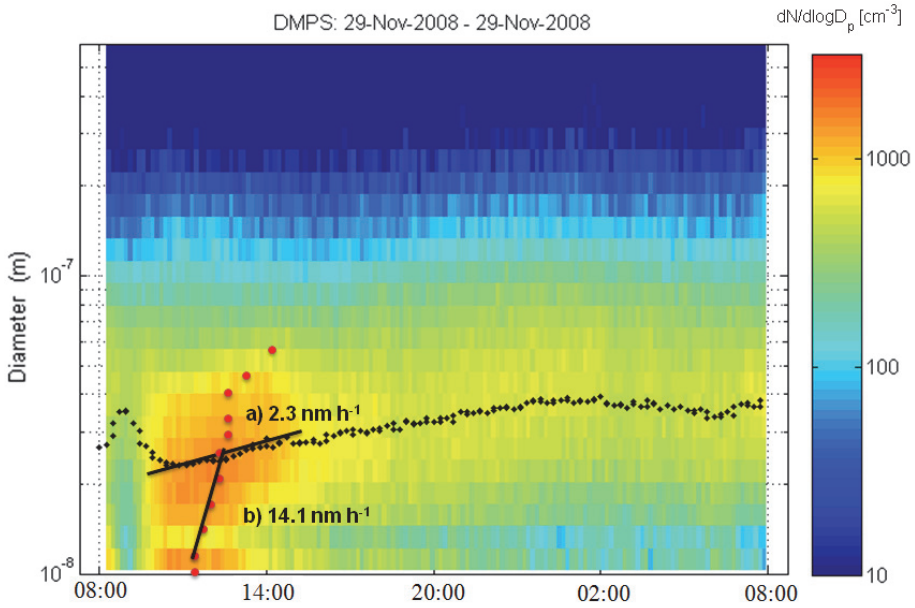

Fig. 9. New particle formation event in 29 November 2008. Black dots represent the calculated geometric mean diameter and red dots the maximum of mode. Black lines are the fitted slopes where growth rate was determined. Slope **(a)** is fitted to the geometric mean and slope **(b)** to the maximum of modes. Both methods seemed to give reasonable looking growth rate, but growth rate **(b)** was used in the analysis. The time axis is in UTC + 08:00.

ACPD
13, 5729–5768, 2013

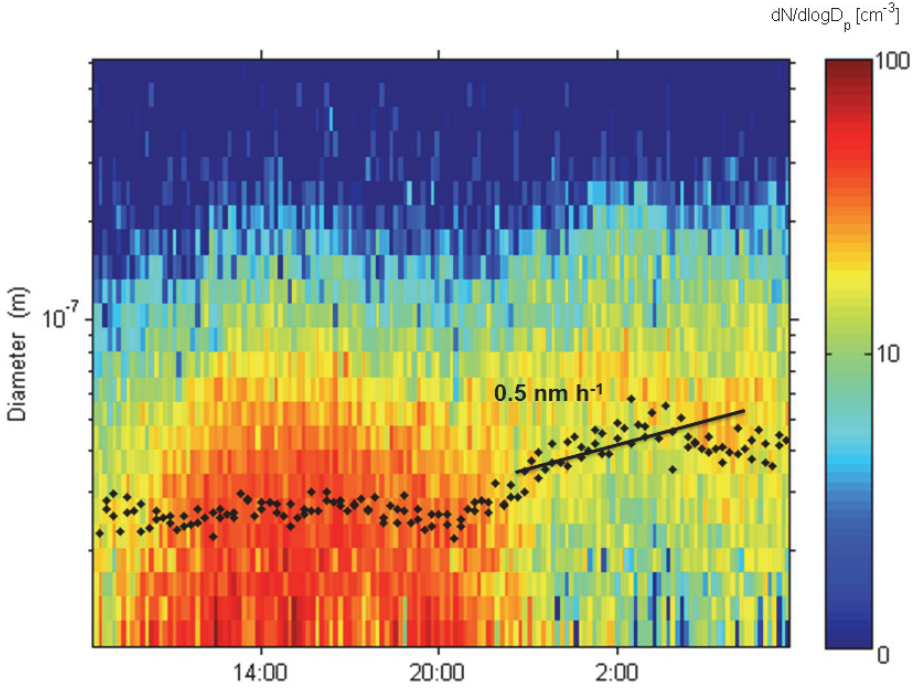

Fig. 10. New particle formation event during dark time in Antarctic winter 11 June 2008. Black dots represent the calculated geometric mean diameter and black line the fitted slope where growth rate for 25–600 nm was determined. Notice the different color scale. The time axis is in UTC + 8.

ACPD
13, 5729–5768, 2013

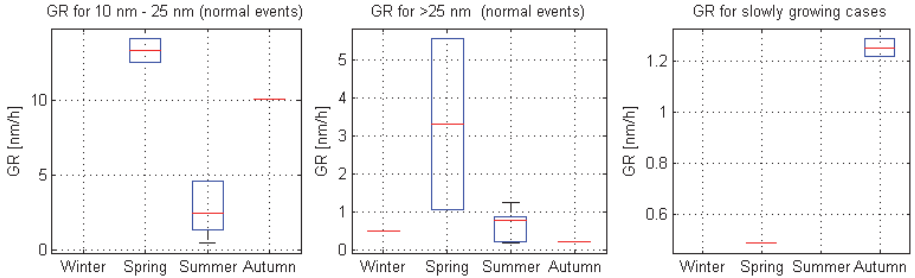

Fig. 11. Growth rate statistics as a function of season. Seasons are winter (June, July, August), spring (September, October, November), summer (December, January, February) and autumn (March, April, May). For normal events in the size class of 10 to 25 nm growth rate statistics for spring were determined from two cases, statistics for summer from 10 cases and statistics for autumn from one case. For normal events in the size class of > 25 nm growth rate statistics for winter were determined from one case, statistics for spring from two cases, statistics for summer from seven cases and in autumn there were only one growth episode from which growth rate was able to be determined. For slowly growing cases growth rate in spring were determined from one case and in autumn there were two slowly growing episodes.

ACPD
13, 5729–5768, 2013

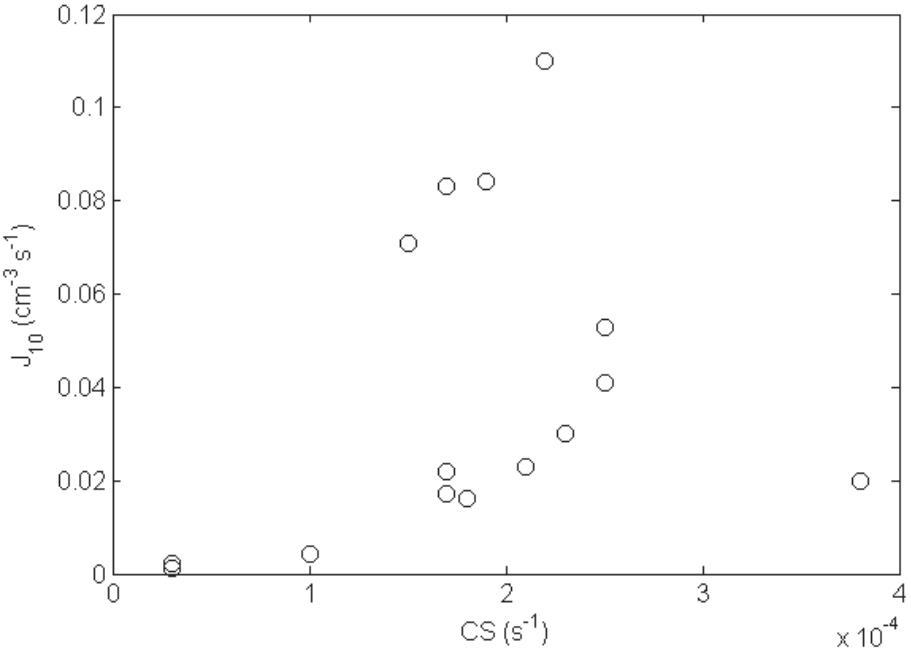

Fig. 12. The formation rate of 10 nm particle as a function of the condensation sink for the class1 events.

ACPD
13, 5729–5768, 2013